

High-brightness ultra-cold metastable neon-beam

Fujio Shimizu

Institute for Laser Science, University of Electro-Communications, 1-5-1
Chofugaoka, Chofu, Tokyo 113-8585, Japan

ABSTRACT

This paper presents detailed characteristics of an ultra-cold bright metastable neon atomic beam which we have been using for atom-interferometric applications. The basis of the device is an atomic beam released from a magneto-optical trap (MOT) which is operated with a high intensity trapping laser, high magnetic quadrupole field, and large laser detuning. An idealized MOT is that atoms stay in a high magnetic-field-seeking state and are reflected back towards inner side by selectively absorbing the laser photon which travels outwards of the trap. In three dimensional configuration, however, an atom has always finite probability to be pumped into a low-field-seeking state, because the direction of the magnetic field and the propagation direction of the laser cannot be parallel in entire space. Furthermore, at the center of the quadrupole field there is no preferred polarization for absorption. Mainly due to those effects a bright small spot of atoms is formed near the center under an appropriate operating condition. We obtained the minimum trap diameter of $50 \mu\text{m}$, the atomic density nearly 10^{13} cm^{-3} , and the atomic temperature slightly less than the Doppler limited temperature of $200 \mu\text{K}$. By releasing trapped atoms we obtained an bright cold atomic beam which is not far from the collision limited atomic density.

1 Introduction

Interferometric manipulation of atoms is still in a primitive stage compared to that of photons. When we try to work with atoms, the most serious problem is that a large inter-atomic interaction limits the atomic density in the beam by many orders of magnitude less than that of photons in an optical beam. The brightness of a classical optical beam is proportional to the inverse of the source area, if the total intensity is the same. The invention of lasers removed this restriction, because in principle the wave front of a laser light can be controlled at will. Bose-Einstein condensate(BEC) of atoms[1, 2] can provide the same benefits for an atomic beam. However, up to now,

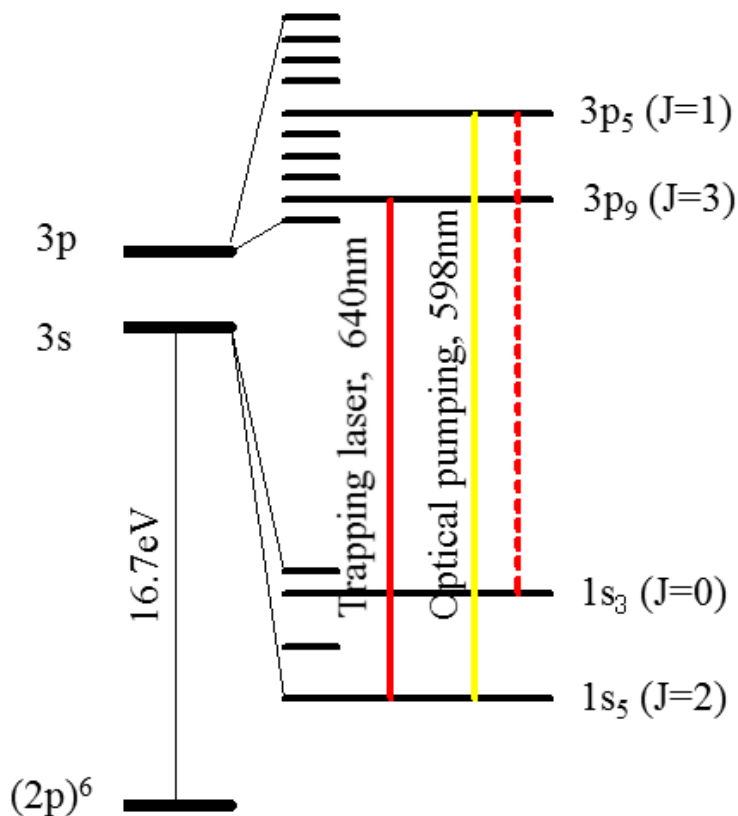


Figure 1: Energy levels of a neon atom relevant to the atomic beam generation. Neon atoms in the $1s_5$ level are laser cooled and trapped using the cyclic transition of $1s_5 - 3p_9$ at 640 nm. The trapped atoms are illuminated by a laser which is resonant to the $1s_5 - 3p_5$ transition. Approximately a half of the $3p_5$ atoms decay to the second metastable state $1s_3$. The remaining half immediately decay to the ground state via two $J = 1$ states by emitting a 70 nm VUV photon. The lifetime of the $1s_5$ and $1s_3$ are approximately 20 s.

an atomic beam generated from BEC is operated only intermittently. In addition, BEC is not a collection of free atoms such as photons of a laser. It is uncertain if the atoms can be expanded to a coherent wave of independent atoms whose wave front can be controlled as intended. Therefore, it seems to be more practical to use the same technique which has been used in classical optics. This is to emit the atomic beam from a small bright source with a small energy dispersion.

The apparatus we describe below uses a "magnetic trap" formed in the magneto-optical trap (MOT)[3], which, we found, is generated stably when MOT is operated with high laser intensity, large detuning, and high magnetic gradient. The atomic species we use is Ne^{20} in the $1s_3$ metastable state which has no magnetic moment $F = 0$. (Fig. 1) First, neon atoms in the $1s_5$ metastable state ($J - 2$) is trapped using a four beam magneto-optical trap[4]. Then, atoms are released continuously from the trap using an optical pumping laser at 597,7 nm that transfers $1s_5$ atoms to the $1s_3$ state via $3p_5(J - 1)$ state. The same technique can be used for other rare gas atoms such as Ar, Kr and Xe.

Examples of the "magnetic trap" which is formed near the $B = 0$ point are shown in Figs 2 and 3. When sufficient number of atoms is fed into the MOT, and the MOT is approximately spherically symmetric, the MOT has a bright spot in the center, and is accompanied by a wing whose intensity decreases roughly inverse to the distance. The size of the MOT generally increases as the detuning of the trapping laser is increased, and its pattern tends to form a ring shape. Even in that situation the "magnetic trap" is frequently observed near the "B=0" point which does not necessarily overlap with the main ring as seen Fig. 3.

In the next section we describe briefly general theoretical considerations on the beam source. In the third section we describe the configuration of our atomic beam apparatus in detail. Then, the experimental results of the atomic trap and beam are given in the following section. A few demonstrative interferometric experiments are given in the last section.

2 Theoretical consideration

Unlike an optical beam, an atomic beam suffers loss of coherence caused by collisions between atoms in the beam. If the diameter of the source is d , and average atomic velocity is v , the atom stays in the source at least $t \geq d/v$. If $v = 0$, it is the time that the gravity pull out the atom from the source, $t \geq \sqrt{2d/g}$, where g is gravitational acceleration, $g = 9.8$ m/s. The

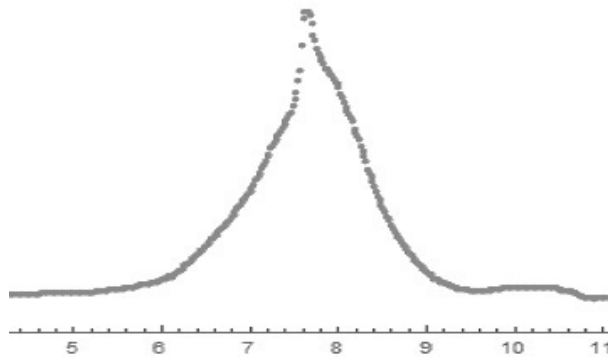
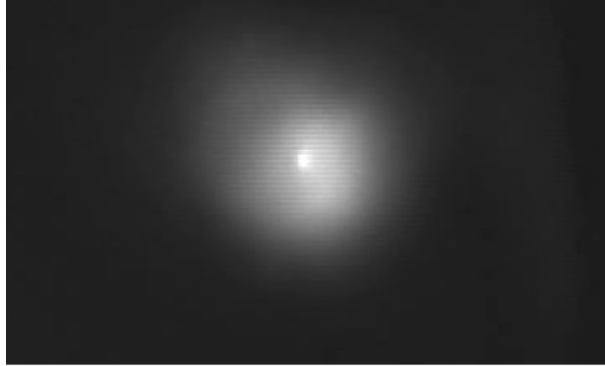


Figure 2: Typical trap pattern (top) and its intensity distribution (bottom) when the feeding of atoms into the MOT is sufficiently strong. When the feeding is weak only the central bright spot is observed. In this figure the brightness of the central spot is saturated. Numbers below the curve is in mm. Neon atoms arrive from left.

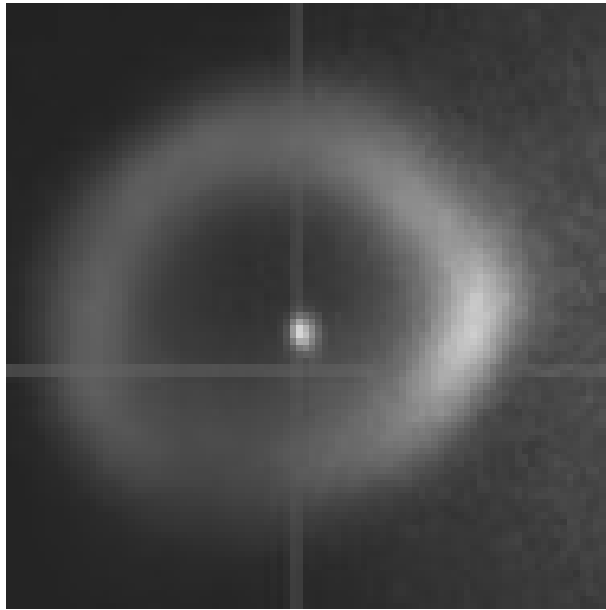


Figure 3: "Magnetic trap" appears not only when the trap pattern is symmetric. When the laser detuning is large, a slight mis-alignment tends to form a ring shape trap. Even in this situation a bright spot around the $B = 0$ point appears frequently. Its position is independent of the main ring as shown in this figure. The size of the figure is 1.8×1.8 mm.

atom has to escape from the source before the coherence is lost by collisions between trapped atoms. Therefore,

$$t \leq \frac{1}{\alpha n}, \quad (1)$$

where α is the two-body collision rate, and n is the density of the atom. Then, the maximum density of the atom is

$$n \leq \frac{v}{\alpha d} \text{ or } \sqrt{\frac{g}{2d\alpha^2}}, \quad (2)$$

and the maximum flow of the atomic beam N is,

$$N = \frac{nd^3}{t} = \frac{v^2d}{\alpha} \text{ or } \frac{gd^2}{2\alpha}. \quad (3)$$

The flux of the atomic beam decreases with d . However, the brightness increases, because it is proportional to d^2 . The flux decreases also with the kinetic energy of the atom. The brightness, however, is constant.

For atoms with a large collision cross sections such as metastable rare gases, the maximum flux N is not large. For $1s_5$ metastable neon the two-body loss rate is $\alpha = 2.5 \times 10^{-10} \text{ cm}^3\text{s}^{-1}$ [6]. The typical values of our source in the best experimental conditions are $v = 20 \text{ cm s}^{-1}$ and $d = 60 \text{ }\mu\text{m}$. Then, the ultimate maximum density is between 10^{13} cm^{-3} and 10^{12} cm^{-3} , and the atomic flow 10^{10} s^{-1} to 10^8 s^{-1} .

In a commonly used MOT, d is much larger than $d = 60 \text{ }\mu\text{m}$. Simple MOT theory tells that the trap size is determined by the surface where atoms in the high-field-seeking magnetic state is resonant to the red-detuned trapping laser. Atoms are assumed to stay dominantly in the high-field-seeking state. This is correct as an approximate physics of MOT, but in actual experiment the situation is much more complex. To keep atoms always in the high-field seeking states, the magnetic field and the k-vector of the optical field must be parallel. This cannot be done in three-dimensional quadrupole field. Therefore, Atom has probability to be pumped to a low-field seeking state, and this is spatially dependent. The intensity of the laser also influences the MOT. If the laser intensity is weak, the atom interacts with the laser only at a large distance from the center of the magnetic quadrupole field. When the intensity is strong, the atom interacts even near the center where there is no preferentially populated magnetic sublevels. The MOT is generally very stable, and can resist against intensity and spatial imbalance of the trapping laser beams. This produces various structure

of atomic cloud which is sometimes difficult to control. Those factors, we believe, creates the bright spot around $B = 0$ point.

Experimentally, when the laser intensity and magnetic field gradient are large, and the laser detuning is large, a small bright spot of very cold atoms near the $B = 0$ point is commonly observed. This is the atomic source we use to generate cold atomic beam, and we call his source as "magnetic trap" in the following sections, though the bright spot may not be the standard magnetic quadrupole trap which works without optical field.

The path of atoms that feed the trap also influences the maximum beam intensity. If the atom moves along a line keeping its diameter, collision rate during the approach is equal to the rate in the trap. Therefore, the maximum beam density is reduced by a ratio between the path length and d . If atoms approach from various direction on a one-dimensional line, the atomic density decreases as $1/r$, where r is the distance from the center. The total loss by binary collision is only logarithmically divergent. If atoms approach two dimensionally, the loss increases only a factor two. The dynamics can be estimated from the fluorescence pattern of the trapped atoms. If atoms approach two dimensionally, the fluorescence intensity is inversely proportional to r provided that their velocity is constant.

3 Neon beam chamber

The vacuum chamber consists of a metastable beam source, a deflector-collimator, a graded Zeeman magnetic field coil to slow metastable atoms, and the MOT region. They are placed horizontally. The experimental chamber is attached vertically below the MOT section. (See Fig. 4.)

The metastable neon atoms are generated by a weak discharge through the sapphire capillary. Its diameter was 0.5 mm, and the length is 5 mm. The sapphire is cooled by liquid nitrogen on contact. (See Fig 5.) This section is pumped by a 800 litter turbo pump and is connected to the downstream through a 3 mm ϕ hole. The neon atoms are led into the deflector-collimator section through this hole. (See Fig 6.)

The collimator consists of two pairs of concave-convex mirrors. Two pairs are placed diagonally so that each pair collimates the two orthogonal radial directions of the beam. The curvature of the mirror are 1.30 m for the convex mirror and 1.38 m for the concave mirror. Two mirrors are placed concentrically. The deflector laser at 640.4 nm is focused at 1.3 m upstream of the inlet of the collimator sets, and is expanded to approximately 20 mm in diameter at the inlet. It is divided into two, and each half is led into

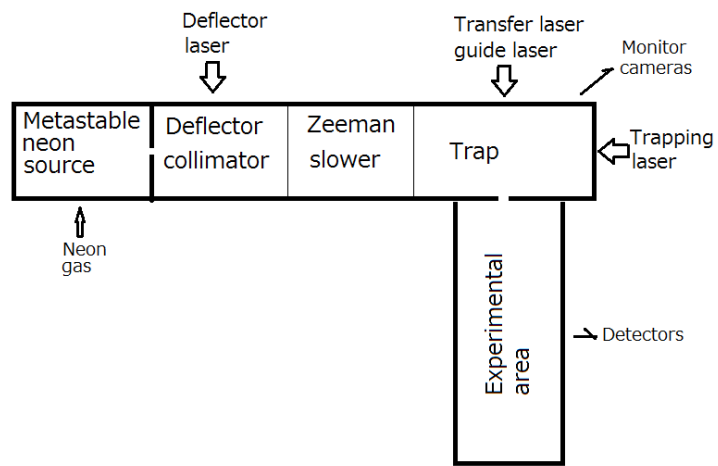


Figure 4: Schematics of the experimental vacuum system. Metastable neon atoms are generated in the source section, travel right, and are trapped in the trap section. Trapped atoms are illuminated by the transfer laser, released from the trap, and fall into the experimental area which is located below the trap section.

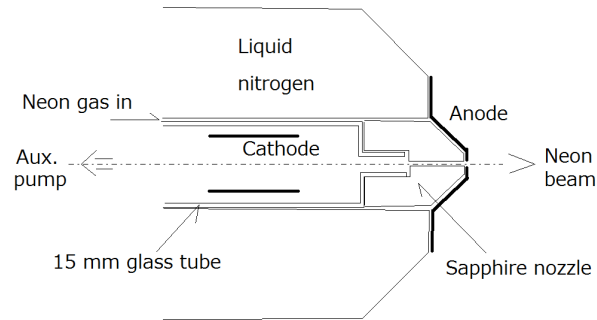


Figure 5: Metastable neon atoms are generated by weak discharge in the sapphire capillary which is cooled by liquid nitrogen. The diameter of the capillary is 0.5 mm, and its length approximately 10 mm. Discharge current is typically 10 mA.

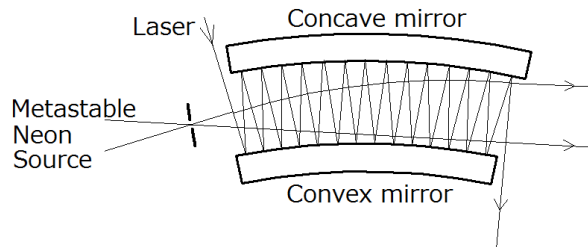


Figure 6: The deflector-collimator. The figure shows one of two mirror pairs. The concave and convex mirrors are placed concentrically. The radii of the curvature are 1.38 and 1.30 meters, respectively. The mirrors are rectangular with the size of 40×150 mm. Another pair of mirrors are placed perpendicular to this pair. The laser beam reflects between two mirrors typically 30 times.

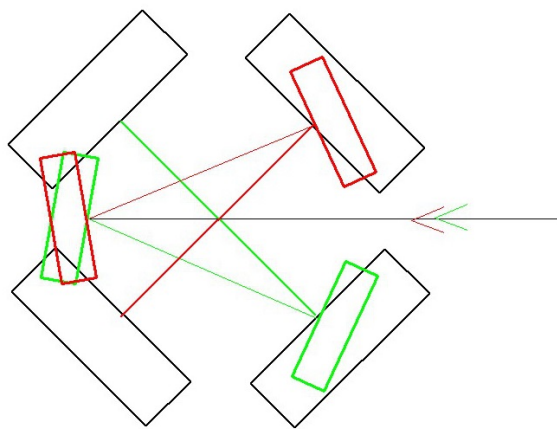


Figure 7: The input mirror configuration of the deflector. The input laser beam is focused at approximately 1.3 m upstream of the inlet. The beam diameter expands to approximately 20 mm at the inlet. The beam is divided into two by two small rectangular flat mirrors, and distributed to each deflector mirror pair (bigger rectangles in the figure). The configuration of the input mirrors equalizes the path length from the pre-focus point to the deflector mirror pairs. The size and pattern of the laser are kept approximately same when the laser travels zigzag between two mirrors.

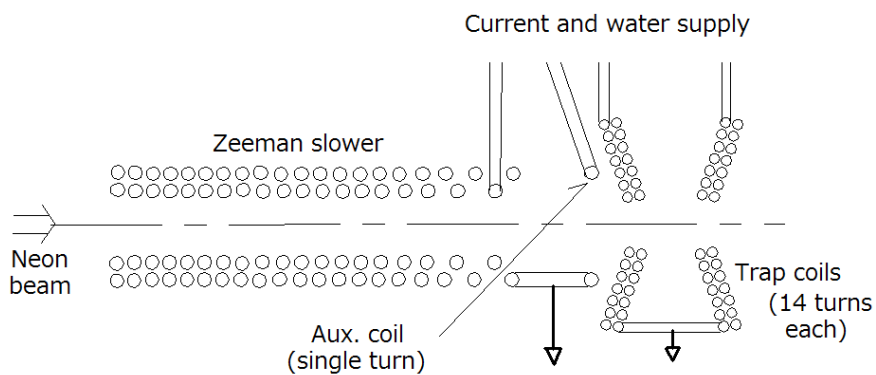


Figure 8: The metastable neon beam enters in the Zeeman coil made of two layers of 3/8 inch copper tube, then, moves to the trap coils which produces a quadrupole magnetic field. A single-turn coil is placed between the Zeeman and trap coils to optimize the beam transfer into the trap. The trap coils are made of 1/8 inch copper tube, The shape of the trap coil is a truncated cone with the apex angle of 142 degrees to allow the trapping laser beams into the center of the quadrupole magnetic field. The current of the Zeeman coil is typically 190 A, The trap coils produce the magnetic field gradient of 1 T/m along the beam axis at 100 A. All coils are cooled by flowing pressurized water typically at 1.7 MPa.

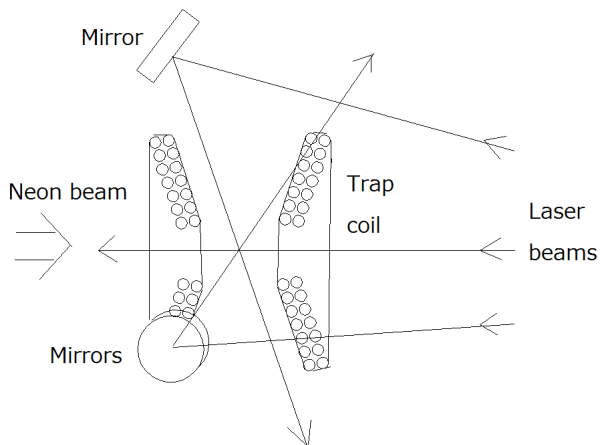


Figure 9: Trap coils. Trap coils are made of 1/8 inch copper tube, and are cooled by pressurized water flow at 1.7 MPa. The figure show top view. The gap between two coils is approximately 4 cm. They produce the magnetic field grating of 1 T/m (along the symmetry axis) with the current of 100 A.

two mirror pairs, respectively. Four rectangular mirrors are used to feed the laser into two mirror pairs keeping the same optical path length. The laser travels zigzag between two mirrors. The number of reflection is typically 30, which can be changed by adjusting the input angle of the laser. The pattern of the laser beam on the mirror is kept approximately same because of the concentric arrangement of convex-concave mirrors and pre-focusing of the laser beam. The system collimates approximately 0.1 radian of the metastable neon beam. This results enhancement of the trapped neon atoms typically by a factor of 50. The frequency stability of the laser required for the efficient collimation was approximately 10 MHz.

Neon atoms are decelerated inside the Zeeman coil which is made of two layers of 3/16 inch copper tube. The length of the coil is approximately 45 cm, and the coil produces axial magnetic field which is maximum at the inlet and decreases to zero at the exit of the coil. (See Fig. 8.) Atoms are then led into the trap coils which produces quadrupole magnetic field with the symmetry axis parallel to the atomic beam direction. Since we use relatively high field gradient for the MOT, a single turn coil is inserted between the Zeeman coil and the trap coil to improve the coupling efficiently of atoms into the trap region. The magnetic field gradient was between 1.5 T/m and 0.4 T/m. All coils are cooled by pressurized water through the

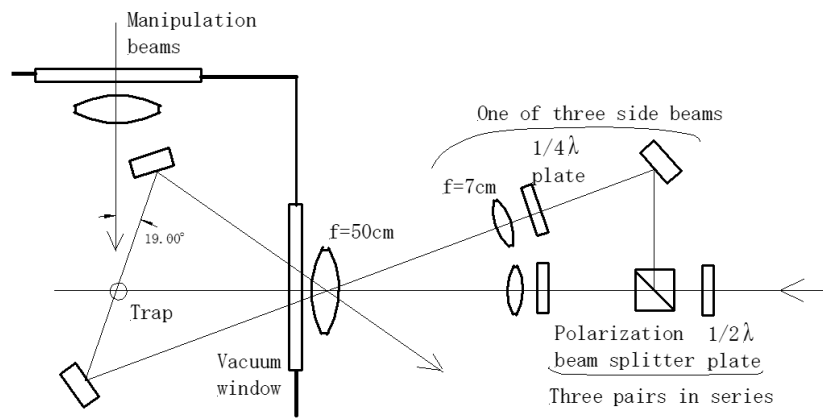


Figure 10: Optical arrangement of the trapping laser beams. The trap laser beam is divided into four beams by three pairs of a half-wave plate and a polarization beam splitter. The three pairs are placed in series along the symmetry axis. Then, four laser beams are circularly polarized of the same polarity, are expanded their radius with two lenses, and led into the trap vacuum chamber, three side beams are directed towards the trap from the backside, and after passing through the trap the second mirror directs the beams outside the vacuum chamber to avoid the laser beams hitting the vacuum chamber wall.



Figure 11: A part of the Zeeman slower. When the deflector-collimator is working, the fluorescence from the metastable neon atoms should be clearly visible.

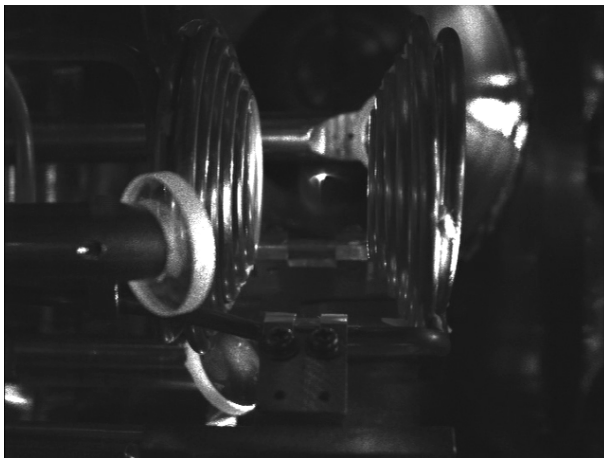


Figure 12: Photo of the trap coils, trapped atoms and a part of the manipulating mirrors for the trapping laser. Atoms come from left.

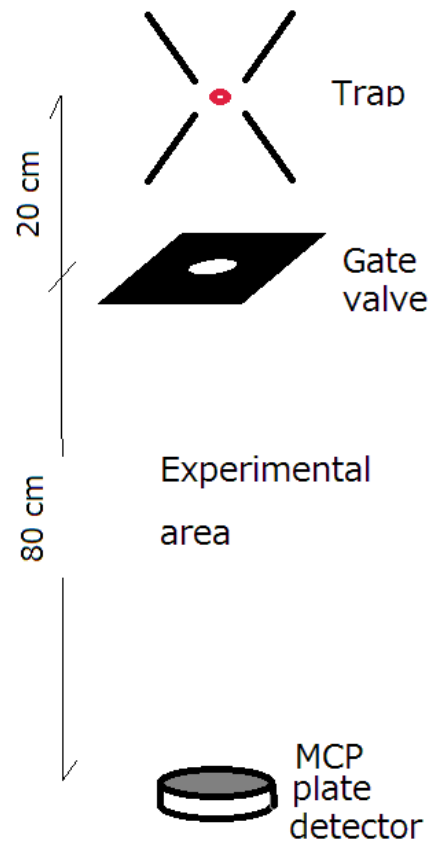


Figure 13: The experimental area. Slow $1s_3$ metastable neon atoms fall vertically. They pass through a racetrack shape gate valve of 5×8 mm which separates the experimental area at 20 cm below the trap. Atoms are detected by a micro-channel detector (MCP) equipped with fluorescent plate, which is placed typically 80 cm below the gate valve. The pressure in the experimental chamber is typically 5×10^{-8} Pa.

copper tube at the pressure of 1.7 MPa. (See Fig. 9).

Figure 11 shows a part of the Zeeman coil. Fluorescence from the trapping laser should be clearly visible when the deflector-collimator is operating properly. Figure 12 is the trap part. The diameter of the mirrors to guide the side laser beams is 19 mm. Typical pressure in the trap region is 3×10^{-7} Pa, when the atomic beam is on.

MOT was achieved by using four laser beams[4]. One laser beam heads towards the beam source, which is parallel to the atomic beam. The remaining three laser beams are shoot at approximately 71 degrees to the atomic beam axis. The optics to distribute trapping beams are shown in Fig. 10. The laser beam at 640 nm from the Coherent 699 dye laser is split into four by using four pairs of half-wave plate and polarization beam splitter. Then, the polarization of each beam is converted to circular of the same polarity with a 1/4 wave plate. Then, they are expanded with two lenses before they are led into the vacuum chamber. The maximum power density of a single beam was approximately 90 mW/cm². The transfer laser beam at 598 nm is focused in the trap from the top. This laser transfers trapped neon atoms in the 1s₅ state to the 1s₃ state by optical pumping and releases atoms from the trap. The released atoms fall vertically into the experimental area.

The experimental area is separated from the rest of the vacuum chamber through a race-track shaped gate valve. This part is a vertically placed 76 cm long 6 inch tube with several ports to insert parts necessary for experiment. Metastable atoms are detected by a micro-channel plate detectors (MCPs) equipped either fluorescence plate or an anode. Typical pressure in this region was 3×10^{-7} Pa. (See Fig. 13.)

4 Experimental results of the trap

We operated the MOT at large magnetic field gradient, high laser intensity, and high laser detuning. The magnetic field gradient was typically 1T/m, and was varied from 0.2 T/m to 1.5 T/m. The laser power density was from 90 mW/cm² to 20 mW/cm², and the detuning up to -120 MHz. Under this operating condition the MOT produced an additional stable trapping region near zero magnetic field point. The temperature of this $B = 0$ trap was usually lower than the Doppler limit temperature[5], and had a small size.

For the standard operating condition of MOT the trap size is expected to increase linearly with the detuning of the trapping laser. Atoms in the high magnetic field seeking state are reflected back at the ellipsoid surface

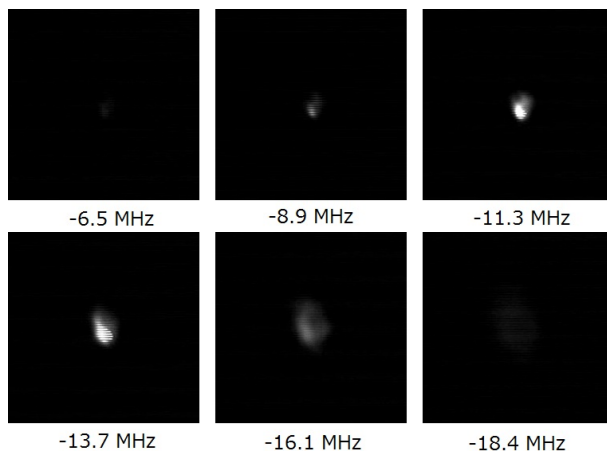


Figure 14: The trap pattern as a function of the detuning of the trapping laser, when operating parameters are in the commonly used range. Laser intensity of each arm is 4 mW/cm^2 . Numbers below each figure is the detuning of the trapping laser. Natural line width of the trap transition, $1s_5 - 2p_9$, is 4 MHz. The size of each picture is $4.6 \times 4.6 \text{ mm}$.

resonant to the cyclic transition $1s_5$ to $2p_9$. The ellipsoid expands linearly with the detuning. Figure 14 shows typical MOT pattern of the trapped atoms with the laser power density of a few times of the saturation intensity and the detuning of a few times of the natural line width. Trap size is seen to increase with the detuning of the laser as expected from this simple theory.

The situation is different when both the laser power and detuning are large, and the magnetic field gradient is large. (See Figs 15 and 16.) We were always able to generate a bright small spot near the $B = 0$ point by adjusting the trap laser direction and intensity. Figures 15 and 16 show trap patterns as a function of laser detuning for weak and strong metastable source intensity, respectively. In Fig. 16 the source intensity is approximately 50 times stronger than in Fig. 15. In each picture the peak intensity rightness is normalized for better visibility of the atomic density profiles. A bright spot around the $B = 0$ point persists up to the detuning of -100 MHz. The field gradient along the symmetry axis is 1 T/m, and the laser intensity of 80 mW/cm^2 for each beam. The minimum diameter is approximately $60 \mu\text{m}$ for the weak source (Fig. 15), and $100 \mu\text{m}$ for the strong source (Fig. 16). As shown in Fig. 17 and 18 the diameter of the trapped atoms do not change much over a wide range of laser detuning. It increases with decreasing

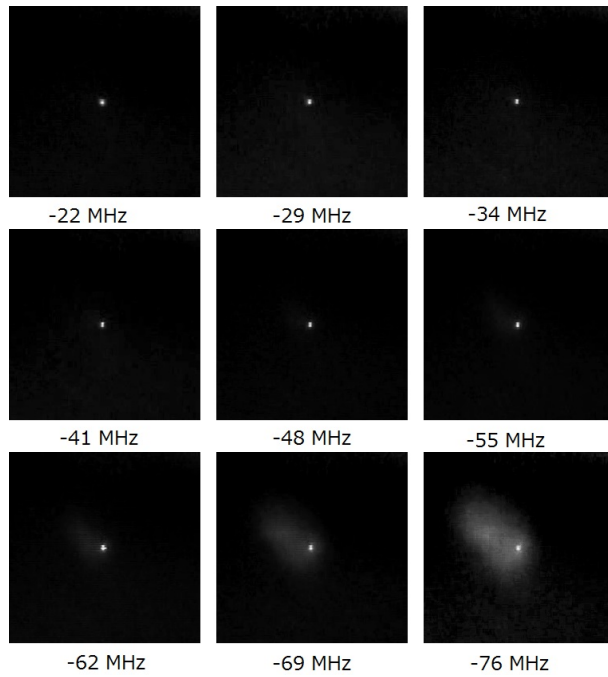


Figure 15: The trap pattern as a function of the detuning of the trapping laser. The number below the figure is the detuning of the trapping laser. For those figures, the deflector-collimator is not in use. Therefore, the source intensity is relatively weak. Bright spot near the zero magnetic field persists over a wide range of detuning. The brightness of the picture is normalized independently in each picture. The size of each picture is 4.6×4.6 mm.

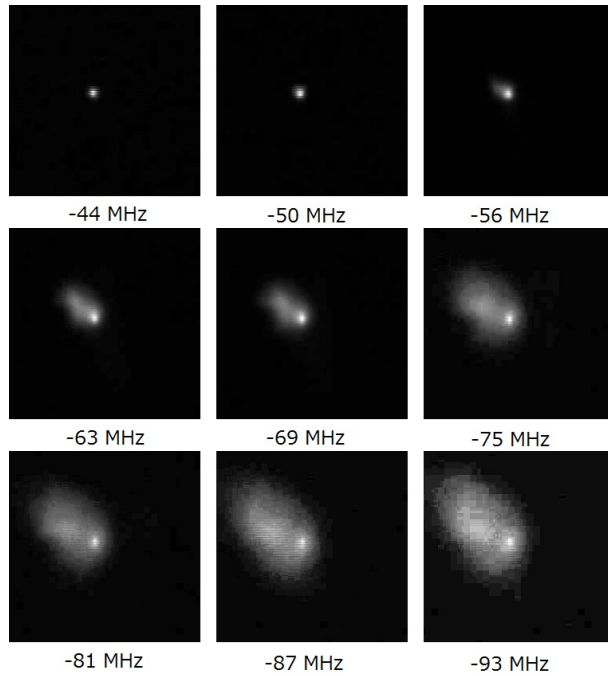


Figure 16: The trap pattern as a function of the detuning of the trapping laser. The number below the figure is the detuning of the trapping laser. Neon beam is collimated after the nozzle. The fluorescence intensity is nearly 100 times stronger than in Fig. 15. The bright spot persists, and it is accompanied by big cloud around the spot. This is due to a shorter lifetime of the bright spot due to high atomic density. The brightness of the picture is normalized independently in each picture. The size of each picture is 4.6×4.6 mm.

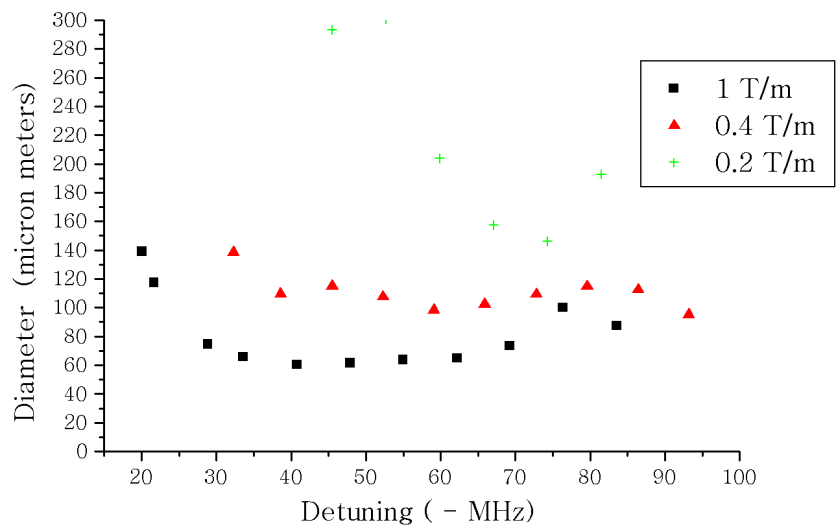


Figure 17: The trap diameter as a function of the detuning of the trapping laser for three quadrupole field intensities. The source intensity is weak. Deflector-collimator is not in operation.

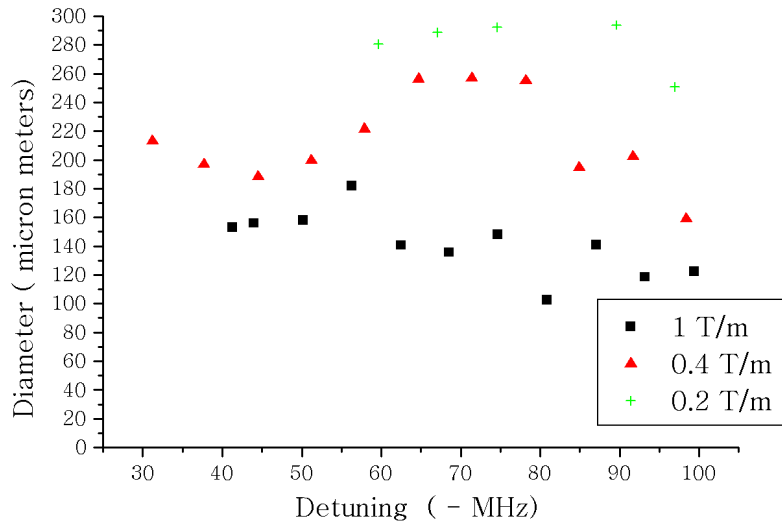


Figure 18: The trap diameter as a function of the detuning of the trapping laser for three quadrupole field intensities. The source intensity is strong. Deflector-collimator is in operation.

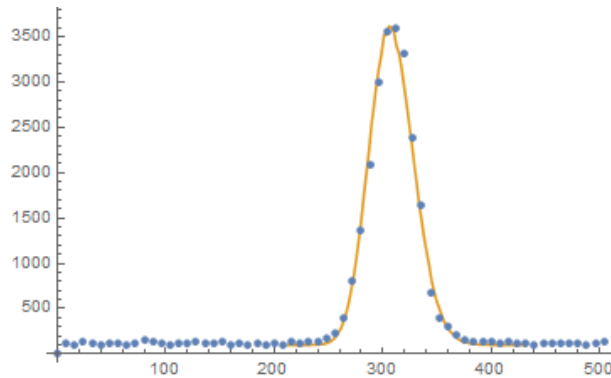


Figure 19: Typical time-of-flight pattern measured with a MCP placed 46 cm below the trap, Abscissa is the time-of-flight from the source to the detector in ms. Ordinate is 100 times of the atom counts in each bin (8 ms wide). The fitting curve is for the 20 cm/s gaussian velocity distribution at the source.

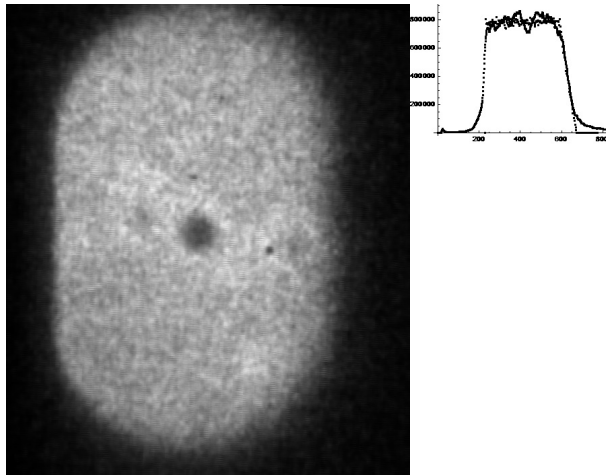


Figure 20: The image of the gate on the micro-channel plate detector(MCP) which is placed 94 cm below the trap. The curve on the right shows horizontal intensity variation. The trap is located near the left edge of the race-track pattern. Therefore, the velocity distribution of the trapped atoms can be estimated from the slope of the right edge. Gray dots shows the curve which is obtained by assuming gaussian distribution of $v = \sqrt{3} \times 30$ cm/s. The exposure time of the figure is 3.3 s. Dark spot near the center is the defect of the MCP. The horizontal size of the picture is 13.5 mm.

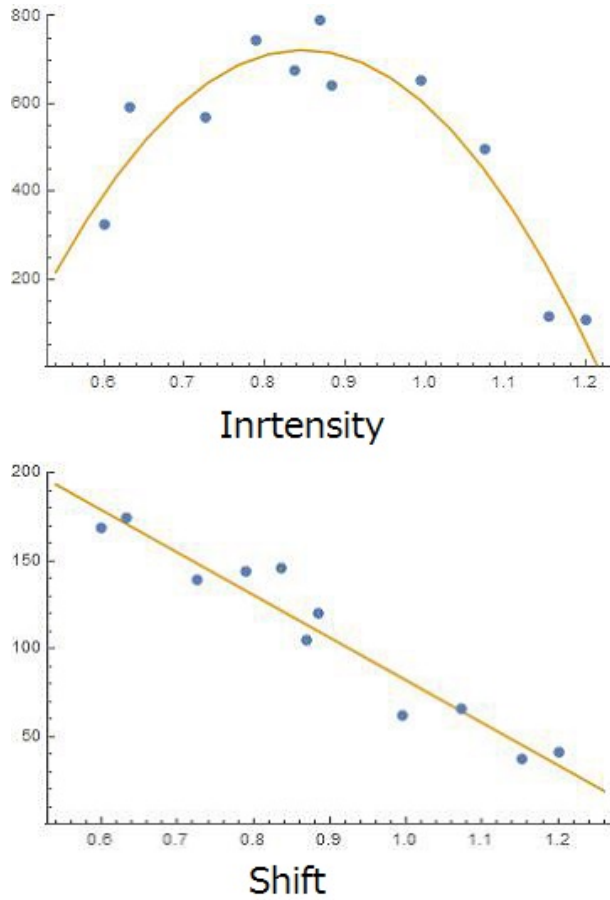


Figure 21: Spatial stability of the trapped atoms. The influence on the trap pattern by the imbalance of trapping laser beams. In this graph, the intensity of three side beams are kept approximately equal, and the intensity of the on axis beam is changed. Abscissa is the intensity ratio between the on-axis and side beams. The ordinate of the lower figure is the relative shift of the trap position in μm . The trap position is seen to move roughly the bright spot diameter.

field gradient. However, the variation is slower than the inverse law. The diameter is larger when the source intensity is strong. This indicates that the temperature of the trap decreases slightly when the field gradient is lower. It is probably hotter when the source intensity is stronger, because atoms stay shorter time in or near the trap before removed by inelastic collisions.

The trapped atoms are released by the transfer laser at 598 nm focused on the bright $B = 0$ spot. The diameter of the laser at the focal point was approximately $30 \mu\text{m}$, and the divergence angle between $1/5$ and $1/10$. The optimal intensity of the transfer laser varies with the atomic density of the bright spot reflecting the collisional lifetime. When the feeding of the atom into the trap was large as shown in Fig. 16, the generated $1s_3$ atomic beam was strongest when the transfer laser was several μW . When the feeding was weak as in Fig. 15, the optimal intensity was in the order of 100 nW . If the intensity of the transfer laser was not excessive, the $1s_3$ atomic beam drew a clear shadow image of the gate valve on the MCP placed at the bottom of the experimental chamber as shown in Fig. 20. We can estimate the atomic velocity distribution at the source. In this figure the horizontal position of the trap was placed close to the left edge of the gate image. Therefore, the slope of the right edge reflects the velocity distribution. The typical velocity obtained by this method is 50 cm/s resulting the temperature of $260 \mu\text{K}$. This method gives higher temperature than the direct measurement described below, probably because it includes the broadening of the edge by the limited resolution of an atom image, the trap size, and other disturbance during the flight.

More accurate measurement was obtained by the time-of-flight measurement (Fig. 19). A short transfer laser (2 ms) illuminated the trap, and the time-of-flight of the released $1s_3$ atoms was detected by a MCP placed at 46 cm below the trap. Typical one-dimensional velocity was 20 cm/s to 30 cm/s , corresponding to the temperature of 45 to $100 \mu\text{K}$. Since the transfer laser was illuminated for a short time and with low-repetition rate, this value shows the temperature of the steady state, where trapped atoms are lost only by inter-atomic collisions.

Another method is to estimate from the diameter of the bright spot. Assuming that this bright spot is practically the magnetic quadrupole trap, its radius can be calculated from the Zeeman shift. The typical radius is $60 \mu\text{m}$ at 1 T/m . The temperature is then $30 \mu\text{K}$, if the atom is in the $M = 1$ level, and $60 \mu\text{K}$, if in the $M = 2$ level of the $1s_5$ state. This result, suggests that the attractive Zeeman force of the quadratic magnetic field plays an important role for the forming of the bright spot near $B = 0$ point.

To test the spatial stability of the bright spot we measured the intensity

and the position of the trap when the relative intensity between the on-axis laser beam and the side beams were varied. Figure 21 shows the result when the intensity of the three side beams were kept approximately equal, and the intensity of the on-axis beam was varied. The trap persisted even when the on-axis beam intensity was varied more than a factor two. In addition the shift of the trap position was in the same order of the trap diameter over the entire intensity range. Furthermore, the trap intensity was maximum when the on-axis laser intensity was slightly less than that of the side beams. At exactly $B = 0$ the force exerted on the atom is that of the molasses[5]. Atoms are not trapped. However, if the favorable condition to the low-field-seeking levels is formed as a result of intensity imbalance, atoms will be trapped as in the case of the magnetic quadrupole trap.

A reliable way to estimate the atomic density in the "magnetic trap" is to analyze the recovery curve of the density of the trapped atoms when the transfer laser is turned off. The recovery curve is given by

$$n(t) = n_f \frac{A \exp t/\tau - 1}{A \exp t/\tau + 1} \quad (4)$$

with $A = (n_f - n_i)/(n_f + n_i)$ and $\tau = 1/(\alpha n_f)$, where n_f is the steady state intensity, n_i is the density when the transfer laser is on, and α is the binary collision rate. For our case $\alpha = 2.5 \times 10^{-10} \text{cm}^3 \text{s}^{-1}$ [6]. We obtained the shortest recovery time of $\tau = 10^{-3}$ s. This gives $n = 4 \times 10^{12} \text{cm}^{-3}$. This value is not far from the maximum density we can expect, which is described in Sec. 2.

5 Numerical simulation

We tried to simulate the experimental results in the previous section by semi-classical numerical simulation. The result justifies only qualitatively our experimental observations that atoms tend to accumulate near $B = 0$ point under some conditions. The calculation uses a simplified semiclassical method in which we assume (1) the atom has definite location and velocity, (2) it moves on the specific quantum state potential, and (3) the atom repeats the following cycle. The atom is initially in the ground state. Then, its upper-state probability increases by the interaction with trapping laser field. When the elapsed time becomes equal to the natural lifetime of the excited state, the atom decays to the ground state by emitting a spontaneous photon. The time evolution of the excited state population is assumed to be

$$|\psi_i(t)|^2 = a\{1 - \exp(-bt)\}^2, \quad (5)$$

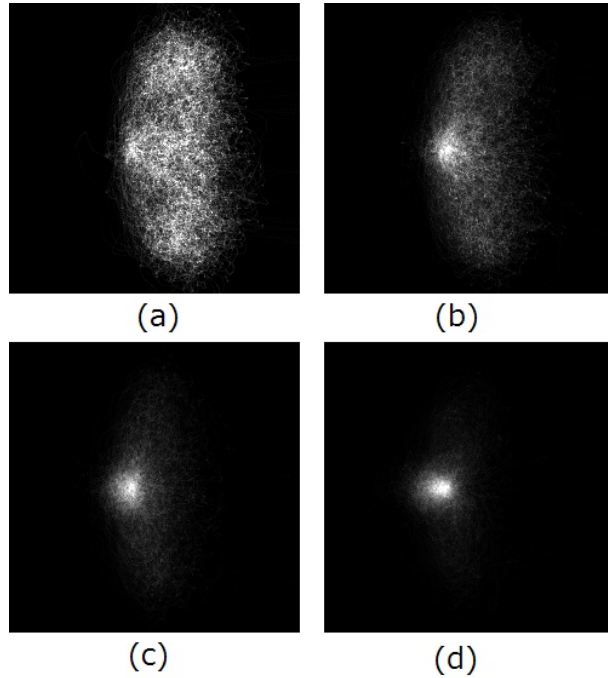


Figure 22: Trap pattern of four-beam MOT. Four figures show the change of the trapped atom pattern when one of the trapping laser intensity is slightly changed. The picture show the pattern accumulated from the trajectory of 50 atoms. (a) The intensity of the four laser beams are equal and 60 times of the saturation intensity. (b) The axial beam is 0.95 times of the other beams. (c) 0.9 times. (d) 0.85 times. The detuning of the laser is 10 times of the natural width. The magnetic field gradient is 10 mT/cm along the atomic beam direction. Atoms fly from right to left. The picture size is 2×2 mm.

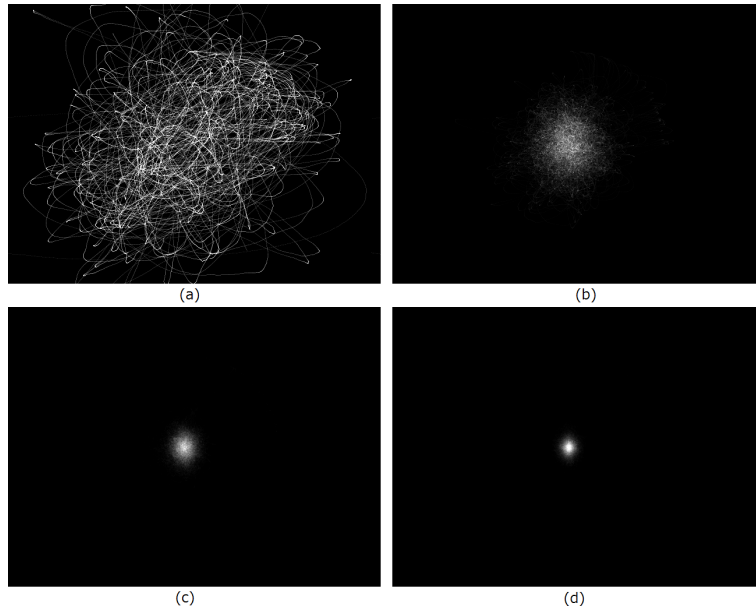


Figure 23: Trap pattern of the standard six-beam MOT. Four figures show the change of the trapped atom pattern with the laser intensity. The pictures show the pattern accumulated from the trajectory of 50 atoms. The intensity of the laser beams is (a) three times of the saturation intensity (b) 10 times (c) 30 times (d) 100 times. The lowest power to form a trap is a little less than three times of the saturation intensity. The detuning of the laser is 10 times of the natural width. The magnetic field gradient is 10 mT/cm along the atomic beam direction. Atoms fly from right to left. The picture size is 3×4 mm.

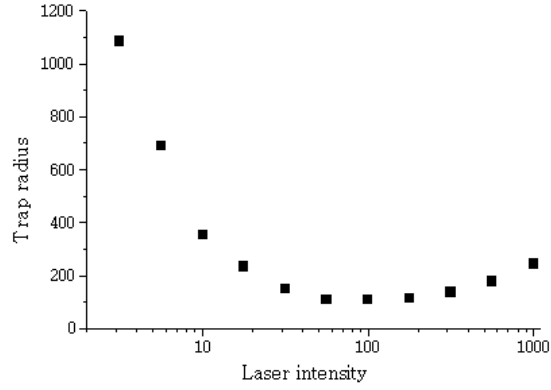


Figure 24: The trap radius vs trap laser intensity. The abscissa is in unit of the saturation power. The ordinate is in unit of μm . The magnetic field gradient is 1 T/m. The laser detuning is 10 times of the saturation intensity.

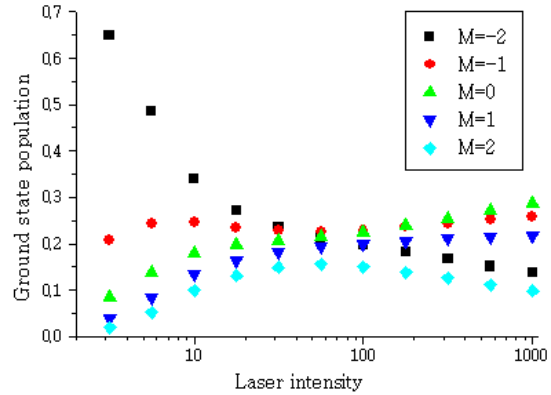


Figure 25: Distribution among magnetic sublevels in the lower state $1s_5$. The abscissa is in unit of the saturation power. The magnetic field gradient is 1 T/m. The laser detuning is 10 times of the saturation intensity.

where a and b are constants determined by the conditions in which $|\psi_i|^2$ is accurate at small t and approaches to the stationary value at large t .

Figure 22 shows an example of the trapped atomic cloud with a four-beam MOT. Four pictures in the figure show the change of the trap pattern as the on-axis laser intensity is changed. When the intensity of all lasers are equal, the trap is large and has elliptical shape. When the intensity of the on-axis laser is slightly reduced relative to the other lasers, atoms start to be accumulated around the $B = 0$ point. As the on-axis intensity is further reduced, the bright spot persists and moves slightly towards downstream. This behavior is qualitatively the same as the experimental observation. However, the stable range of the bright spot is less than that observed in the experiment.

Though we do not have experimental verification, the four laser beam configuration is probably not the necessary condition to produce the $B = 0$ spot. Figure 23 shows the trap pattern when the laser intensity is changed from near threshold to 100 times of the saturation intensity for the standard six-beam MOT. Together with Fig. 24 the influence of the laser intensity is dramatic. The diameter shrinks as the laser intensity increases towards the saturation intensity at the $B = 0$ point. It is clear from Fig. 25 that the population is more or less equally populated among all magnetic sublevels around the saturation intensity.

6 Optical dipole guide

Since the transverse velocity is conserved, the atomic beam radius expands as it falls down. The atomic beam can be compressed by guiding the beam with a laser red-detuned to the $1s_3 - 3p_5$ transition. We overlapped a red-detuned laser on the transfer laser. The red-detune laser was focused to the same spot as the focal point of the transfer laser (see Fig. 26). this red-detuned laser cools the transverse momentum of atoms in the beam, and increases the atomic density in the beam up to several orders of magnitude. Its function depends on the divergence and the intensity of the laser. When the laser is tightly focused, falling atoms feel radially expanding potential, and are cooled its radial motion. When the radius at the focal point is sufficiently large, the laser will keep its radius for a long distance, and the atom is trapped inside the laser beam.

Figure 27a shows typical MCP images of the shadow of the gate for various operation conditions. C is the image obtained by a weak atomic source, B shows the case of strong source, where the deflector-collimator

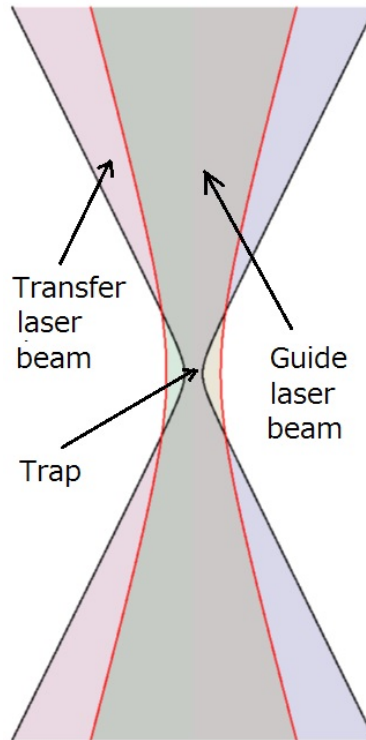


Figure 26: Transverse cooling of the atomic beam. The diameter of the transfer laser is approximately $30 \mu\text{m}$ at the focal point. The diameter of the guide laser can be equal or larger than that of the transfer laser. When the diameter is larger, the neon beam is guided inside the laser beam for a long distance. When small, the transverse velocity of the neon beam is adiabatically cooled, and the neon atoms are released quickly from the guide laser potential.

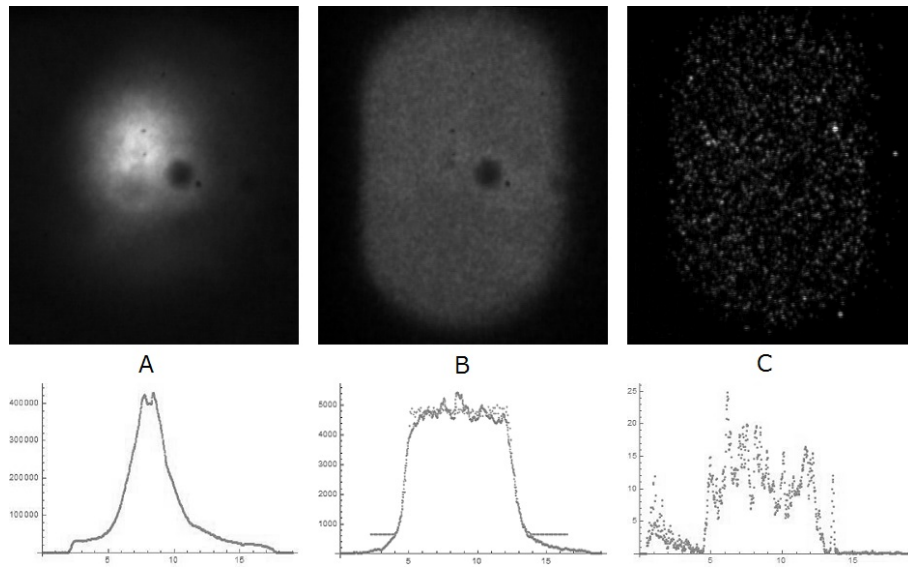


Figure 27: Atomic beam pattern on the MCP. A: Pattern with the optical dipole guide. The deflector laser is on to increase the metastable beam intensity. B: optical dipole guide is turned off from A. C: both dipole guide and deflector lasers are off. The brightness of each picture is independently adjusted. The bottom curves show the intensity variation along the horizontal direction around the center. Ordinates show the real intensity ratio among the three pictures. Abscissa is in mm. Exposure time of pictures are 30 s.

is used. In Fig. A optical dipole laser focuses the $1s_3$ atomic beam. The ordinate of the graphs in the lower part shows the actual intensity ratio. From C to A, the atomic beam intensity increases almost a factor of 10^4 .

7 Example of diffraction pattern

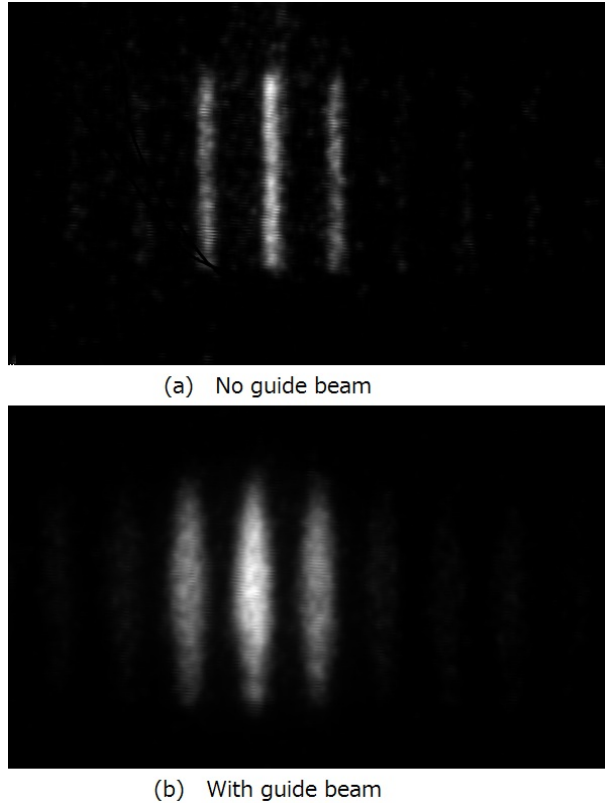
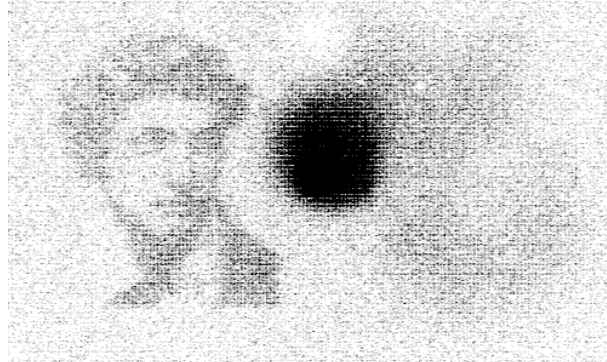
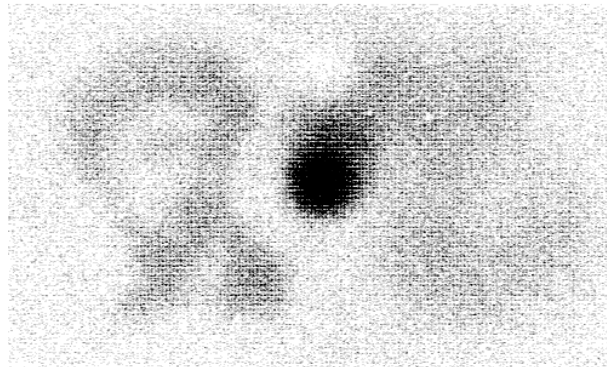


Figure 28: The zero-th and ± 1 -st order diffraction patterns from a grating. The grating size is 3×0.2 mm, Its pitch is $2 \mu\text{m}$ with $1 \mu\text{m}$ slit. For a simple pattern such as this diffraction from a grating, the interferometric image can be recognized by real time video. When the atomic beam is guided by laser, the image broadens, because the effective source size increases. The exposure time is 5 s.

We show in this section two interferometric patterns obtained with our atomic beam described in the previous sections. Figure 28 shows the zero-th



(a) No guide beam



(b) With guide beam

Figure 29: The holographic pattern of reference [8]. (a) is without dipole guide, and (b) is with dipole guide. The exposure time is 120 min for (a), and 30 min for (b). The hologram size is $800 \mu\text{m}$ square with 20 % opening. To obtain diffraction pattern much more complicated than Fig. 28, a long exposure time is necessary. Furthermore, the image is degraded if the transverse cooling by an optical-dipole guide is used, due to the increased effective source size as shown in (b). Meshes seen in the figure is artifacts of the video software(s).

and \pm first order diffraction patterns from a narrow grating. For a simple interferometric pattern like this case a single video frame of 1/30 s exposure time is sufficient to recognize gross pattern. For a more complicated pattern such as the image from the computer generated holographic image in Fig 29 relatively long accumulation time is necessary. Furthermore, degradation of the source quality harms the quality of the picture as shown in Fig. (b), which uses the guide laser to increase the atomic beam intensity.

8 Discussion

Since metastable rare gas atoms can be detected with a high quantum efficiency, they are ideal atomic species for the demonstration of interferometric phenomena. Unfortunately, metastable rare gas atoms have a large inelastic collision rate. We demonstrated a bright neon atomic beam in the $1s_3$ metastable state. Atoms are released from the "magnetic trap" which is formed near the center of quadrupole magnetic field of a MOT. At this moment we do not know the precise dynamics of the trapped atoms, such as, the range of atoms which is collected by the "magnetic trap", and how they are cooled to the observed temperature. More precise analysis of dynamics may bring to the generation of better cold atomic beams.

Another interesting experiment is to try with atoms which have smaller inelastic collision rate. Application of known other cooling techniques may bring a brighter cold atomic beam, or even finding of new collective phenomena.

Acknowledgements

The author would like to thank Prof. J. Fujita for supplying us the holographic film of Giuliano de Medici (Fig. 29). Its pattern was calculated by Prof. T. Kishimoto.

References

- [1] M.H. Anderson, J.R. Ensher, M.R. Matthews, C.E. Wieman, and E.A. Cornell, "Observation of Bose-Einstein condensation in a dilute atomic vapor", *Science*, **269**, 198 (1995).

- [2] K.B. Davis, M.O. Mewes, M.R. Andrews, N.J. Vandruten, D.S.Durfee, D.M. Kurn, and W. Ketterle, "Bose-Einstein condensation in a gas of sodium atoms", Phys. Rev. Lett. **75**, 3969 (1995).
- [3] E. L. Raab, M. Prentiss, Alex Cable, Steven Chu, and D. E. Pritchard, "Trapping of Neutral Sodium Atoms with Radiation Pressure", Phys. Rev. Lett. **59**, 2631 (1987).
- [4] F. Shimizu, K. Shimizu, and H. Takuma, "Four-Beam Laser Trap of Neutral Atoms", Opt. Lett. **16**, 339 (1991).
- [5] Steven Chu, L. Hollberg, J. E. Bjorkholm, Alex Cable, and A. Ashkin, "Three-dimensional viscous confinement and cooling of atoms by resonance radiation pressure", Phys. Rev. Lett. **55**, 48 (1985).
- [6] P. Spoden, M. Zinner, N. Herschbach, W. J. van Drunen, W. Ertmer, and G. Birkl, "Collisional Properties of Cold Spin-Polarized Metastable Neon Atoms", Phys. Rev. Lett. **94**, 223201 (2005).
- [7] F. Shimizu, K. Shimizu, and H. Takuma, "Double-Slit Interference with Ultra-cold Metastable Neon Atoms", Phys. Rev. A, **46**, R17, (1992).
- [8] T. Kishimoto, J. Fujita, S. Mitake, and F. Shimizu, "Gray-scale atom holography", Jpn. J. Appl. Phys. **38** , L683 (1999).